Numerical analysis of Burgers' equation with uncertain boundary conditions using the stochastic Galerkin method

Per Pettersson*, Gianluca Iaccarino†, Jan Nordström‡

March 31, 2008

Abstract

Burgers' equation with stochastic initial and boundary conditions is investigated by a polynomial chaos expansion approach where the solution is represented as a series of stochastic, orthogonal polynomials. The analysis of wellposedness for the stochastic Burgers' equation follows the pattern of that of the deterministic Burgers' equation.

We use dissipation and spatial derivative operators satisfying the summation by parts property and weak boundary conditions to ensure stability. Similar to the deterministic case, the time step for hyperbolic stochastic problems solved with explicit methods is proportional to the inverse of the largest eigenvalue of the system matrix. The time step naturally decreases compared to the deterministic case since the spectral radius of the continuous problem grows with the number of polynomial chaos coefficients.

Analysis of the characteristics of a truncated system gives a qualitative description of the development of the system over time for different initial and boundary conditions. Knowledge of the initial and boundary expected value and variance is not enough to get a unique solution. Also, the sign of the polynomial chaos coefficients must be known.

The deterministic component (expected value) of the solution is affected by the modeling of uncertainty. A shock discontinuity in a purely deterministic problem can be made smooth by assuming uncertain boundary conditions.

*Division of Scientific Computing, Department of Information Technology, Uppsala University, Sweden.

†Center for Turbulence Research, Department of Mechanical Engineering, Stanford University, USA.

‡Division of Scientific Computing, Department of Information Technology, Uppsala University, Sweden.

1 Introduction

Many physical problems are subject to uncertainty in parameter values, input data or even in the geometry of the physical domain of the problem. This has given rise to the need for uncertainty quantification of the output data. Fields of application of uncertainty quantification include turbulence, climatology [17], turbulent combustion [18], flow in porous media [7] and fluid mixing [27].

Uncertainty quantification is in a broad sense the qualitative and quantitative analysis of uncertainty in a general decision problem. Accurate decisions require uncertainty quantification to be accompanied by verification of the agreement between expected results and results predicted by the model and validation to ensure that the measured quantities agree with the intended use of the model. Uncertainty quantification is a prerequisite for making correct decisions [3].

Uncertainty is characterized as either *aleatory*, i.e. due to natural randomness, or *epistemic* which means it is caused by lack of knowledge. The latter kind of uncertainty can be reduced by more accurate measurements and models, whereas aleatory uncertainty is partly intrinsic to the problem and cannot be reduced completely. Aleatory uncertainty can be quantified by the use of probabilistic models. Epistemic uncertainty can also be quantified in this way if model improvement is not feasible.

An example of the need for uncertainty quantification in applications related to methods and problems studied in this report is the investigation of the stability properties of an airfoil. Uncertainty in physical parameters such as structural frequency and initial pitch angle affect the probability of limit cycle oscillations. The method of *polynomial chaos* has been used to obtain statistical stability limits and calculate the risk for system failure [23, 2].

Although of limited practical use in fluid mechanics applications, the Burgers' equation is an interesting and highly non-linear model problem and many results can be extended to other hyperbolic problems, such as the Euler equations. In this project, uncertainty quantification will be performed for the stochastic Burgers' equation by a spectral representation in the form of polynomial chaos expansion of the solution. The equation is stochastic in the sense of uncertainty in the initial and boundary values. Stochastic Galerkin projection of the stochastic Burgers' equation results in a deterministic system of equations from which the expected values and variance of the solution can be determined.

In order to ensure stability of the discretized system of equations, *summation by parts* operators and weak imposition of boundary conditions [14, 15, 5] are used to obtain energy estimates. The system is expressed in a split form that combines the conservative and non-conservative formulation [13]. A particular set of artificial dissipation operators [12] and penalty matrices affecting the boundaries are used to enhance the stability close to the shock. Burgers' equation has been discretized with a fourth order central difference operator in space and the fourth order Runge-Kutta method in time.

There are several approaches to uncertainty modeling in numerical simulations.

Compared to the Monte Carlo method where a vast number of simulations are performed, only one simulation is performed with the polynomial chaos approach. However, the system of equations that has to be solved grows with the order of polynomial chaos and the dimension of the stochastic input.

An increased number of Monte Carlo simulations implies a statistical solution at a higher confidence level. For any level of confidence in the polynomial chaos approach, one single simulation is sufficient and the number of polynomial chaos coefficients is independent of the confidence level. However, the accuracy of this solution is dependent on the number of polynomial chaos coefficients.

The polynomial chaos method is generalized in the sense of [24], i.e. a general framework allowing for the use of different polynomial bases to quantify uncertainty from various sources and probability distributions. However, the original Hermite polynomial basis is chosen as the model basis in this report. The polynomial chaos approach is a non-statistical method since only one simulation is required to evaluate the polynomial chaos coefficients that determine the solution at every point in space and time, as well as expected value and variance.

A third approach to model uncertainty is perturbation methods where the perturbed solution is Taylor expanded in the proximity of the original solution. This approach is only accurate for small perturbations, i.e. variance small compared to the expected value [1, 25].

Yet another way of quantifying uncertainty is by using the Karhunen-Loève expansion which involves spectral expansion of the covariance function. This results in fast convergence but requires knowledge of the covariance function which is generally not available. For further reading, see [11].

Studies have been performed on the location of the transition layer of a shock discontinuity arising in simulations of the Burgers' equation with non-zero viscosity. Small one-sided perturbations imply large variation in the location of the transition layer, so-called *supersensitivity* [26], which is a problem in deterministic as well as stochastic simulations. The results from the polynomial chaos approach are accurate and the method is faster than the standard Monte Carlo method [25, 26]. Burgers' equation with a stochastic force term has been investigated and compared to standard Monte Carlo methods [10].

In addition to the more general problem of a system growing with the number of polynomial chaos coefficients, the following special problems exist.

- Divergence due to singularities in the probability space. Convergence requires the probability space to be smooth [21].
- Long-term integration resulting in accuracy decreasing with time [16, 21].

The long-term integration problem is due to the transition to higher order polynomial chaos modes with increasing time which implies that the truncation error increases with time. Linear dependence between the required number of polynomial chaos coefficients and simulation time for a given order of accuracy is shown

in [21]. This holds for problems involving random frequency, which are not of the same kind as the problems of main interest in this survey.

One way of overcoming problems of this kind is to use multi-element generalized polynomial chaos in which polynomial chaos is implemented element-wise for a decomposition of the random space. Another method is Wiener-Haar expansion, where the usual global Askey polynomial basis is replaced by a basis of Haar wavelets [16].

2 Polynomial chaos expansion

The theoretical foundations underlying polynomial chaos was first formulated in [22]. The solution to the partial differential equation is expressed as a spectral expansion of a second order random field

$$u(x,t,\xi) = \sum_{i=0}^{\infty} u_i(x,t)\Psi_i(\xi), \tag{1}$$

with the inner product

$$\langle u, v\rangle = \int_{\Omega} uvf(\xi)d\xi, \tag{2}$$

where $f(\xi)$ is the probability density function. The solution is subject to the constraint

$$\|u\|^2 = \int_{\Omega} u^2 f(\xi)d\xi < \infty, \tag{3}$$

i.e. second-order random field (finite variance).

Expected values $E(u)$ and variance $Var(u)$ can be expressed as functions of the polynomial chaos coefficients. We have

$$E(u) = \int_{\Omega} \sum_{i=0}^{\infty} u_i\Psi_i f(\xi)d\xi = u_0 \int_{\Omega} f(\xi)d\xi + \int_{\Omega} \sum_{i=1}^{\infty} u_i\Psi_i f(\xi)d\xi = u_0, \tag{4}$$

and

$$\sigma^2 = Var(u) = E[u^2] - (E[u])^2 = \int_{\Omega} \sum_{i=0}^{\infty} u_i^2\Psi_i^2 f(\xi)d\xi - u_0^2 = \sum_{i=1}^{\infty} u_i^2\langle\Psi_i^2\rangle. \tag{5}$$

Based on expected values and variance, confidence intervals for the solution can be written as

$$u(x,t) = u_0 \pm z\sigma \tag{6}$$

where the parameter z depends on the confidence level.

By the Cameron-Martin theorem the solution converges in the L_2 sense [4]. In a probabilistic setting the Cameron-Martin theorem implies mean square convergence, that is

$$\lim_{M\to\infty} E\left[|u - \sum_{i=1}^{M} u_i\Psi_i|^2\right] = 0.$$

Observe that although the solution to Burgers' equation might be discontinuous in the spatial variable, the polynomial chaos coefficients are smooth and converge, see [6].

The basis polynomials $\Psi_i(\xi)$ are orthogonal polynomials of the stochastic variable ξ, and thus

$$\langle \Psi_i, \Psi_j \rangle = \delta_{ij} c_i \tag{7}$$

where c_i is a constant depending on the polynomial basis. The relations between different polynomial bases is described by the *Askey scheme*. For further reading, see for instance [24]. Here it is sufficient to notice that the optimal basis in terms of convergence is Hermite polynomials for Gaussian random input and Legendre polynomials for uniformly distributed random variables. See the appendix for a table of Hermite basis polynomials.

2.1 Polynomial chaos expansion of Burgers' equation

The polynomial chaos representation $u(x,t,\xi) = \sum_{i=0}^{\infty} u_i \Psi_i(\xi)$ is inserted into the Burgers' equation,

$$u_t + u u_x = 0,\ 0 \leq x \leq 1 \tag{8}$$

which yields

$$\sum_{i=0}^{\infty} \frac{\partial u_i}{\partial t} \Psi_i(\xi) + \left(\sum_{j=0}^{\infty} u_j \Psi_j(\xi) \right) \left(\sum_{i=0}^{\infty} \frac{\partial u_i}{\partial x} \Psi_i(\xi) \right) = 0. \tag{9}$$

A stochastic Galerkin projection is performed by multiplying (9) by $\Psi_k(\xi)$ for non-negative integers k and integrating over the probability domain Ω. The orthogonality of the basis polynomials then yields a system of deterministic equations. By truncating the number of polynomial chaos coefficients to a finite number M, the solution is projected from an infinite dimensional probabilistic space onto a finite dimensional deterministic space.

$$\frac{\partial u_k}{\partial t} \langle \Psi_k^2 \rangle + \sum_{i=0}^{M} \sum_{j=0}^{M} u_i \frac{\partial u_j}{\partial x} \langle \Psi_i \Psi_j \Psi_k \rangle = 0 \qquad \text{for } k = 0, 1, ..., M. \tag{10}$$

2.2 Modeling the solution with Hermite polynomials

For a Gaussian distributed input, the optimal polynomial chaos basis with respect to convergence is the set of Hermite polynomials. In this project the probabilistic basis has been used since it is the most intuitive choice with regard to weight function and calculation of expected value and variance. The appendix includes a table of probabilistic Hermite polynomials. The weight function of the inner products is the probability density function of the Gaussian distribution. This means that the inner product of two variables u and v coincides with the expected value of their product.

$$\langle u, v \rangle = \int_{\Omega} uv f(\xi) d\xi = E(uv).$$

For probabilistic Hermite polynomials $H(\xi)$ of Gaussian variables ξ the double inner product defined in (7) is given by

$$\langle H_i H_j \rangle = \delta_{ij} i! \tag{11}$$

The triple inner product in the probabilistic setting is

$$\langle H_i H_j H_k \rangle = \begin{cases} 0 & \text{if } i+j+k \text{ is odd or } \max(i,j,k) > s \\ \frac{i!j!k!}{(s-i)!(s-j)!(s-k)!} & \text{otherwise} \end{cases} . \tag{12}$$

This formula can be derived from a formula in [20] for the triple product of physical Hermite polynomials.

2.3 Truncated system for Burgers' equation

The system of equations resulting from the stochastic Galerkin projection can be written in non-conservative matrix form as

$$H u_t + A(u) u_x = 0, \tag{13}$$

where H is a positive definite constant diagonal matrix with the inner products of the basis polynomials and $A(u)$ is a symmetric matrix depending on u. As an illustration, the 3×3 system given by truncating the expansion to $M = 2$ with a Hermite polynomial basis for Burgers' equation is

$$\begin{pmatrix} 1 & 0 & 0 \\ 0 & 1 & 0 \\ 0 & 0 & 2 \end{pmatrix} \begin{pmatrix} u_0 \\ u_1 \\ u_2 \end{pmatrix}_t + \begin{pmatrix} u_0 & u_1 & 2u_2 \\ u_1 & u_0 + 2u_2 & 2u_1 \\ 2u_2 & 2u_1 & 2u_0 + 8u_2 \end{pmatrix} \begin{pmatrix} u_0 \\ u_1 \\ u_2 \end{pmatrix}_x = 0.$$

From the system of equations it is clear that if no uncertainty is introduced in the polynomial chaos expansion of the initial and boundary conditions, all coefficients $u_i = 0$, $\forall i \geq 1$ and the system is reduced to the scalar, deterministic Burgers' equation. The deterministic Burgers' equation is thus a special case of the stochastic Burgers' equation.

2.4 System in conservation form

Burgers' equation (8) can be expressed in conservation form which will give correct shock speed and is used in the simulations. Burgers' equation in conservative form is

$$u_t + \frac{\partial}{\partial x} f(u) = 0, \tag{14}$$

where $f(u) = u^2/2$. Both the conservative and the non-conservative formulations will be used in following sections.

The polynomial chaos expansion truncated to M terms gives

$$\sum_{i=0}^{M} \frac{\partial u_i}{\partial t}\Psi_i + \frac{\partial}{\partial x}\frac{1}{2}(\sum_{i=0}^{M} \Psi_i u_i)(\sum_{j=0}^{M} \Psi_j u_j) = 0. \tag{15}$$

A stochastic Galerkin projection is performed, yielding

$$\langle \Psi_k^2 \rangle \frac{\partial u_k}{\partial t} + \frac{\partial}{\partial x}\frac{1}{2}\sum_{i=0}^{M}\sum_{j=0}^{M} u_i u_j \langle \Psi_i \Psi_j \Psi_k \rangle = 0, \tag{16}$$

for $k = 0, 1, ..., M$. Note that (16) is in conservative form. In matrix form with the matrices A and H defined as before, this system can be written

$$Hu_t + \frac{\partial}{\partial x} f(u) = 0, \;\; f(u) = \frac{1}{2}A(u)u. \tag{17}$$

As a comparison, the system $u_t + uu_x = 0$ would be written as

$$Hu_t + A\frac{\partial}{\partial x}u = 0. \tag{18}$$

Note that the matrix $A = A(u)$ occurs in both the conservative and non-conservative form.

2.5 Diagonalized system of Burgers' equation

For various purposes, such as analysis of well-posedness, design of dissipation operators and analysis of characteristics, the system of equations (13) is diagonalized. A and H are both positive definite and symmetric matrices and it can be shown that $H^{-1}A$ has real valued eigenvalues and eigenvectors. See [8] for further details and proof.

Let Λ denote a diagonal matrix with the eigenvalues λ_i of $H^{-1}A$ on the main diagonal and V a matrix where the columns are the linearly independent eigenvectors. (13) is written

$$u_t + V\Lambda V^{-1}u_x = 0. \tag{19}$$

Set $w = V^{-1}u$. Multiplication by V^{-1} gives

$$V^{-1}u_t + V^{-1}V\Lambda V^{-1}u_x = 0 \Leftrightarrow w_t + \Lambda w_x = 0, \tag{20}$$

which is diagonal. Assuming non-zero eigenvalues, Λ can be split according to the sign of its eigenvalues as $\Lambda = \Lambda^+ + \Lambda^-$. Introducing the split scheme into the system of equations gives

$$w_t + \Lambda^+ w_x + \Lambda^- w_x = 0. \tag{21}$$

This form will be used in the following sections.

2.6 Multi-dimensional uncertainty

In this section, the concept of uncertainty is extended to multi-dimensional stochastic variables. The stochastic variables are supposed to be independent. For simplicity, only the 2-D case is investigated. Orthogonal 2-D Hermite polynomials are constructed as in the 1-D case. The first few of them are given by:

$$\Psi_0 = 1,\ \Psi_1 = \xi_1,\ \Psi_2 = \xi_2,\ \Psi_3 = \xi_1\xi_2,\ \Psi_4 = \xi_1^2 - 1,\ \Psi_5 = \xi_2^2 - 1.$$

Because of independence, $f_i(\xi_1, \xi_2) = f_{i,1}(\xi_1) f_{i,2}(\xi_2)$. The solution u can then be expressed as

$$u(x,t,\xi_1,\xi_2) = \sum_{i=0}^{M} u_i(x,t)\Psi_i(\xi_1,\xi_2) = \sum_{i=0}^{M} u_i(x,t)\Psi_{i1}(\xi_1)\Psi_{i2}(\xi_2). \tag{22}$$

In analogy with the 1-dimensional case, an inner product is defined as

$$\begin{aligned}\langle \Psi_i \Psi_j \rangle = \int_{-\infty}^{\infty}\int_{-\infty}^{\infty} f_{\xi_1}(\xi_1) f_{\xi_2}(\xi_2)\Psi_i\Psi_j d\xi_1 d\xi_2 = \\ = \int_{-\infty}^{\infty}\int_{-\infty}^{\infty} \frac{1}{2\pi} e^{-\frac{\xi_1^2+\xi_2^2}{2}} \Psi_i\Psi_j d\xi_1 d\xi_2.\end{aligned} \tag{23}$$

The Burgers' equation expressed in this basis truncated to a fourth order expansion is given by

$$\begin{pmatrix} 1 & 0 & 0 & 0 \\ 0 & 1 & 0 & 0 \\ 0 & 0 & 1 & 0 \\ 0 & 0 & 0 & 1 \end{pmatrix} \begin{pmatrix} u_0 \\ u_1 \\ u_2 \\ u_3 \end{pmatrix}_t + \begin{pmatrix} u_0 & u_1 & u_2 & u_3 \\ u_1 & u_0 & u_3 & u_2 \\ u_2 & u_3 & u_0 & u_1 \\ u_3 & u_2 & u_1 & u_0 \end{pmatrix} \begin{pmatrix} u_0 \\ u_1 \\ u_2 \\ u_3 \end{pmatrix}_x = 0. \tag{24}$$

3 Well-posedness of the stochastic Burgers' equation

A problem is *well posed* if the solution exists, is unique and depends continuously on the problem data. An initial-boundary-value problem given by

$$\begin{array}{lll} u_t + H_{op}(x,t,\frac{\partial}{\partial x_i})u = F(x,t) & x \in \Omega & t \geq 0 \\ u = f(x) & x \in \Omega & t = 0 \\ Lu = g(t) & x \in \Gamma & t \geq 0 \end{array} \tag{25}$$

is *strongly well posed* if the solution exists, is unique and is subject to

$$\|u\|_\Omega^2 + \int_0^t \|u\|_\Gamma^2 \, d\tau \leq K_c e^{\eta_c t}\left(\|f\|_\Omega^2 + \int_0^t \|F\|_\Omega^2 + \|g\|_\Gamma^2 \, d\tau\right). \tag{26}$$

K_c and η_c are independent of F, f and g. See [9] [13] for more details.

3.1 The constant coefficient case

In this section we will show that the stochastic Burgers' equation with constant coefficients is well-posed if correct boundary conditions are given. The system is diagonalized and split according to the sign of the eigenvalues as in (21). Multiplying the system (21) with $w^T = (V^{-1}u)^T$ and integrating over the spatial domain yields

$$\int_\Omega (w^T w_t + w^T \Lambda^+ w_x + w^T \Lambda^- w_x) dx = 0. \tag{27}$$

Let the norm over Ω be defined as

$$\|w\|_\Omega^2 = \int_0^1 w^T w dx.$$

Addition of the transposes to (27) leads to

$$\frac{\partial}{\partial t} \|w\|_\Omega^2 = - \left[w^T \Lambda^+ w + w^T \Lambda^- w \right]_0^1. \tag{28}$$

Let w_0 and w_1 denote the values of w at the boundaries. Integration from time 0 to t yields

$$\|w\|_\Omega^2 = \|f\|_\Omega^2 + \int_0^1 \left[-w_1^T (\Lambda^+ + \Lambda^-) w_1 + w_0^T (\Lambda^+ + \Lambda^-) w_0 \right] d\tau. \tag{29}$$

Boundary conditions are imposed on the incoming characteristic variable which corresponds to Λ^+ for $x = 0$ and Λ^- for $x = 1$. On the left boundary, the conditions are set such that $(V^{-1}u)_i = (g_0)_i$ if $\lambda_i > 0$ and on the right boundary $(V^{-1}u)_i = (g_1)_i$ if $\lambda_i < 0$. With known data at the boundaries we get

$$u(x = 0) = g_0 \Rightarrow w_0 = V^{-1} g_0 = \tilde{g_0}$$

$$u(x = 1) = g_1 \Rightarrow w_1 = V^{-1} g_1 = \tilde{g_1}.$$

These boundary conditions are substituted into (29). Adding $\int_0^t (-w_1^T \Lambda^- w_1 + w_0 \Lambda^+ w_0) d\tau$ to both sides and rearranging terms gives

$$\begin{aligned} \|w\|_\Omega^2 + \int_0^t \left(w_1^T \Lambda^+ w_1 - w_0^T \Lambda^- w_0 - w_1^T \Lambda^- w_1 + w_0 \Lambda^+ w_0 \right) d\tau = \\ = \|f\|_\Omega^2 + 2 \int_0^t \left(-w_1^T \Lambda^- w_1 + w_0 \Lambda^+ w_0 \right) d\tau = \\ = \|f\|_\Omega^2 + 2 \int_0^t \left(-\tilde{g}_1^T \Lambda^- \tilde{g}_1 + \tilde{g}_0^T \Lambda^+ \tilde{g}_0 \right) d\tau. \end{aligned} \tag{30}$$

Based on the last equation, the boundary norm is defined as

$$\|w\|_\Gamma^2 = w^T \Lambda^+ w - w^T \Lambda^- w = w^T (\Lambda^+ + |\Lambda^-|) w = w^T |\Lambda| w \text{ for } x = 0, 1.$$

The definition above does not take into account the occurence of eigenvalues equal to zero. If these occur the norm will actually be a semi-norm (since $\|w\| = 0 \Rightarrow w = 0$ does not hold for all cases). Equation (30) now becomes

$$\|w\|_\Omega^2 + \int_0^t \|w_0\|_\Gamma^2 + \|w_1\|_\Gamma^2 \, d\tau \leq \|f\|_\Omega^2 + 2\int_0^t \|\tilde{g_0}\|_\Gamma^2 + \|\tilde{g_1}\|_\Gamma^2 \, d\tau. \tag{31}$$

By setting $K_c = 2$ and $\eta_c = 0$ this is in the form (26).

Uniqueness follows directly from (31). Assume u and v are two different solutions to the Burgers' equation with given conditions. Then $u - v$ is a solution to the homogeneous system. The energy estimate (31) with zero data shows that this solution equals zero everywhere and therefore $u = v$ and the solution is unique. Since existence is trivial in this case (a hyperbolic problem with correct number of boundary conditions), we have shown well-posedness.

The solution of the system of equations for Burger's equation require initial and boundary conditions, determined by the corresponding polynomial chaos coefficients. These coefficients depend on the expected conditions and the distribution of the uncertainty introduced to the system. The stochastic Galerkin technique is used to determine the polynomial chaos coefficients for the initial and boundary values.

As an illustration of the analysis above, consider Burgers' equation with the periodic boundary conditions given by

$$\begin{aligned} &u(0,t) = u(1,t) = 0.1\xi \\ &u(x,0) = sin(2\pi x) + 0.1\xi \\ &\xi \in N(0,1) \end{aligned} \tag{32}$$

The polynomial chaos coefficients for the boundaries are obtained by multiplying by $H_j(\xi)$ for $j = 0, 1, ...$ and integrating over the domain of ξ. Orthogonality of the basis polynomials gives

$$\begin{aligned} &u_0(0,t) = u_0(1,t) = 0 \\ &u_1(0,t) = u_1(1,t) = 0.1 \\ &u_i(0,t) = u_i(1,t) = 0 \qquad \forall i > 1 \end{aligned}$$

These values are inserted into the system matrix A. The signs of the eigenvalues of A determine the number of boundary conditions to be specified. In a similar manner as for the boundary values, the polynomial chaos coefficients of the initial values are calculated

$$\begin{aligned} &u_0(x,0) = sin(2\pi x) \\ &u_1(x,0) = 0.1 \end{aligned}$$

Well-posedness is guaranteed since the polynomial chaos coefficients of the boundary and initial conditions are bounded. The norms in (31) are defined for the polynomial chaos coefficient vectors. In this example,

$$f = (sin(2\pi x), 0.1, 0, ..., 0), \; g_0 = g_1 = (0, 0.1, 0, ..., 0).$$

The problem can now be uniquely solved. Observe that a problem of this kind, with expected zero flow at the boundaries, will have both positive and negative eigenvalues on both boundaries since the flow is equally likely in the direction out from the domain as in the opposite direction. Figure 1 shows the solution at time $t = 0.25$ for this problem truncated to $M = 4$. The variance reaches its peak at the transition layer, which is natural since a small deviation in the shock location results in a large deviation of the solution values in this region.

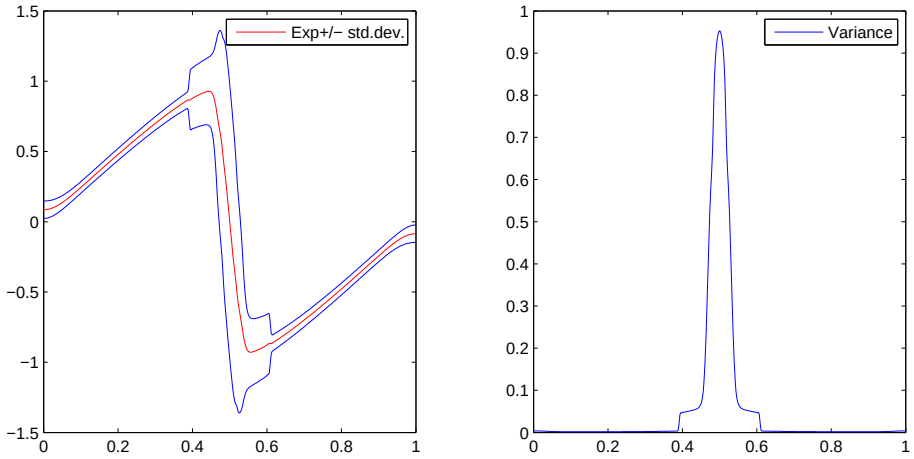

Figure 1: Perturbed sine wave. Expected value and variance at $t = 0.25$. $\sigma = 0.1$ on the boundaries. $E[u] \pm \sigma$ (left) and σ^2 (right).

The convergence of the polynomial chaos expansion is investigated by measuring the discrete Euclidean error norm of the variance and the expected value. For a discretization with m spatial grid points, we have

$$\|\epsilon_{Exp}\|^2 = \frac{1}{m-1}\sum_{i=1}^{m}(E[u_m] - E[u_{ref}])^2$$

and

$$\|\epsilon_{Var}\|^2 = \frac{1}{m-1}\sum_{i=1}^{m}(Var[u_m] - Var[u_{ref}])^2.$$

The analytical solution is generally unknown and therefore a polynomial chaos expansion of high order is used as reference solution (u_{ref}).

M	0	1	2	3	4	5
$\|\epsilon_{Exp}\|$	0.00085	0.00015	0.00012	0.000092	0.000061	0.000030
$\|\epsilon_{Var}\|$	0.0040	0.000078	0.000011	0.0000098	0.0000065	0.0000032

Table 1: Convergence for the solution in Figure 1. u_{ref} for $M = 6$.

As a complement to the investigation of convergence for different number of polynomial chas coefficients, grid convergence is investigated by successively refining the spatial grid size. Since the analytical solution is unknown, the solution for the finest grid (800 spatial points) is used as a reference solution. M is fixed and the norm is measured coefficient wise

$$\|\epsilon_u\|^2 = \frac{1}{m-1}\sum_{i=1}^{m}\sum_{j=0}^{M}((u_j)_i - u_{ref})^2.$$

m	100	200	400
$\|\epsilon_u\|$	0.04272	0.001570	0.0004444

Table 2: Grid convergence for the solution in Figure 1. u_{ref} for $m = 800$ spatial points with fourth order accurate discretization of the spatial derivative.

3.2 The non-linear case

Consider the continuous problem in split form

$$Hu_t + \beta\frac{\partial}{\partial x}(\frac{A}{2}u) + (1-\beta)Au_x = 0,\ 0 \leq x \leq 1.$$

Multiplication by u^T and integration over the spatial domain yields

$$\int_0^1 u^T H u_t dx + \beta\int_0^1 u^T\frac{\partial}{\partial x}(\frac{A}{2}u)dx + (1-\beta)\int_0^1 u^T A u_x dx = 0.$$

Integration by parts gives

$$\frac{1}{2}\frac{\partial}{\partial t}\|u\|_H^2 = -\frac{\beta}{2}[u^T A u]_{x=0}^{x=1} + \frac{\beta}{2}\int_0^1 u_x^T A u dx - (1-\beta)\int_0^1 u^T A u_x dx. \tag{33}$$

We choose β such that

$$\frac{\beta}{2} - (1-\beta) = 0 \Leftrightarrow \beta = \frac{2}{3},$$

which is inserted into (33), yielding

$$\frac{\partial}{\partial t}\|u\|_H^2 = -\frac{2}{3}[u^T A u]_{x=0}^{x=1}. \tag{34}$$

If the boundary conditions derived for the linear problem are used, the problem will be well-posed.

4 Energy estimates for stability analysis

Although the problems of interests are stochastic, the problem that arises from the stochastic Galerkin projection is strictly deterministic. For such a problem, well-known numerical techniques can be used to ensure stable and accurate solutions.

4.1 Summation by parts operators

Summation by parts (SBP) is the discrete equivalence to integration by parts. A difference operator $P^{-1}Q$ has the SBP property if it has the characteristic features

$$Q + Q^T = \begin{pmatrix} -1 & & & & 0 \\ & 0 & & & \\ & & \ddots & & \\ & & & 0 & \\ 0 & & & & 1 \end{pmatrix} \text{ and } P = P^T > 0. \tag{35}$$

P is the so-called diagonal norm. SBP operators are used for approximations of spatial derivatives. Their usefulness lies in the possibility of expressing energy decay in terms of known boundary values, exactly as in the continuous case [19, 12].

Consider the problem $u_t + u_x = 0$ which in the semi-discrete case is

$$u_t + P^{-1}Qu = 0 \tag{36}$$

where $P^{-1}Q$ is a central difference operator approximating the first derivative. All space derivative operators used here can be written in the form $P^{-1}Q$, where P, Q are defined above.

The model problem (36) is multiplied by $u^T P$. Addition of transpose and using the SBP properties (35) yields

$$\frac{d}{dt} \|u\|_P^2 = -u^T(Q + Q^T)u = u_{x=0}^2 - u_{x=1}^2, \tag{37}$$

where $\|u\|_P^2 = u^T P u$. The energy growth is thus totally determined by the boundary values, exactly as in the continuous case.

4.2 Stability of the semi-discretized problem

Consider the continuous problem in non-conservative form

$$Hu_t + Au_x = 0.$$

We will use the so-called *penalty technique* [12] to impose boundary conditions for the discrete problem.

In the analysis below, let $E_0 = (e_{ij})$ where $e_{11} = 1, e_{ij} = 0, \forall i, j \neq 1$ and $E_n = (e_{ij})$ where $e_{nn} = 1, e_{ij} = 0, i, j \neq n$. Define the block diagonal matrix A_g where the diagonal blocks are the symmetric matrices $A(u(x))$. With penalty matrices Σ_0 and Σ_1 corresponding to the left and right boundaries respectively, the discretized system can be expressed as

$$\begin{aligned}(I \otimes H)u_t + A_g(P^{-1}Q \otimes I)u = (P^{-1} \otimes I)(E_0 \otimes \Sigma_0)(u - g_0) + \\ + (P^{-1} \otimes I)(E_n \otimes \Sigma_1)(u - g_1).\end{aligned} \tag{38}$$

Similarly, the conservative system,

$$Hu_t + \frac{1}{2}\frac{\partial}{\partial x}(Au) = 0,$$

can be discretized as

$$(I \otimes H)u_t + \frac{1}{2}(P^{-1}Q \otimes I)A_g u = (P^{-1} \otimes I)(E_0 \otimes \Sigma_0)(u - g_0) + \\ + (P^{-1} \otimes I)(E_n \otimes \Sigma_1)(u - g_1). \quad (39)$$

Neither of the formulations (38) nor (39) will lead to an energy estimate. However, the non-conservative and conservative forms can be combined to get an energy estimate by using the summation by parts property.

A linear combination of the conservative and the non-conservative form is used for the energy estimates, just as in the continuous case, see section 3.2. The split form is given by

$$(I \otimes H)u_t + \beta\frac{1}{2}(P^{-1}Q \otimes I)A_g u + (1-\beta)A_g(P^{-1}Q \otimes I)u = \\ = (P^{-1} \otimes I)\left[(E_0 \otimes \Sigma_0)(u - g_0) + (E_n \otimes \Sigma_1)(u - g_1)\right]. \quad (40)$$

With multiplication by $u^T(P \otimes I)$ the system can be written as

$$u^T(P \otimes H)u_t + \frac{\beta}{2}u^T(Q \otimes I)A_g u + (1-\beta)u^T(P \otimes I)A_g(P^{-1}Q \otimes I)u = \\ = u^T(E_0 \otimes \Sigma_0)(u - g_0) + u^T(E_n \otimes \Sigma_1)(u - g_1). \quad (41)$$

We will use the commutativity property

$$A_g = (P \otimes I)A_g(P^{-1} \otimes I). \quad (42)$$

We add the transpose to (41) and use (42) to get

$$\frac{\partial}{\partial t}\|u\|^2_{(P\otimes H)} + \frac{\beta}{2}u^T\left((Q \otimes I)A_g + A_g(Q^T \otimes I)\right)u + \\ + (1-\beta)u^T\left(A_g(Q \otimes I) + (Q^T \otimes I)A_g\right)u = \\ = 2u^T(E_0 \otimes \Sigma_0)(u - g_0) + 2u^T(E_n \otimes \Sigma_1)(u - g_1). \quad (43)$$

We choose β such that

$$\frac{\beta}{2} = 1 - \beta \Leftrightarrow \beta = \frac{2}{3}.$$

By the summation by parts property (35) this yields the desired form

$$\frac{\partial}{\partial t}\|u\|^2_{(P\otimes H)} = \frac{2}{3}\left(u^T_{x=0}Au_{x=0} - u^T_{x=1}Au_{x=1}\right) + 2u^T_{x=0}\Sigma_0(u_{x=0} - g_0) + \\ + 2u^T_{x=1}\Sigma_1(u_{x=1} - g_1). \quad (44)$$

Restructuring (44) yields

$$\frac{\partial}{\partial t}\left\|u\right\|^2_{(P\otimes H)} = u^T_{x=0}(\frac{2}{3}A + 2\Sigma_0)u_{x=0} - 2u^T_{x=0}\Sigma_0 g_0 - \\ - u^T_{x=1}(\frac{2}{3}A - 2\Sigma_1)u_{x=1} - 2u^T_{x=1}\Sigma_1 g_1. \quad (45)$$

Stability is achieved by a proper choice of the penalty matrices Σ_0 and Σ_1. For that purpose A is split according to the sign of its eigenvalues as

$$A = A^+ + A^- \text{ where } A^+ = x^T\Lambda^+ x \text{ and } A^- = x^T\Lambda^- x. \quad (46)$$

Choose Σ_0 and Σ_1 such that $\frac{2}{3}A^+ + 2\Sigma_0 = -\frac{2}{3}A^+ \Leftrightarrow \Sigma_0 = -\frac{2}{3}A^+$ and $\frac{2}{3}A^- - 2\Sigma_1 = \frac{2}{3}A^- \Leftrightarrow \Sigma_1 = \frac{2}{3}A^-$. We now get the energy estimate

$$\frac{\partial}{\partial t}\left\|u\right\|^2_{(P\otimes H)} = -\frac{2}{3}(u_{x=0} - g_0)^T A^+(u_{x=0} - g_0) + \frac{2}{3}\left[u^T_{x=0}A^- u_{x=0} + g_0^T A^+ g_0\right] \\ - \frac{2}{3}\left[u^T_{(x=1)}A^+ u_{(x=1)} + g_1^T A^- g_1\right] + \frac{2}{3}(u_{(x=1)} - g_1)^T A^-(u_{(x=1)} - g_1), \quad (47)$$

which shows that the system is stable.

5 Artificial dissipation operators

An artificial dissipation operator is essentially a discretized even order derivative. Dissipation operators are added so that the total spatial difference operator becomes one-sided close to the shock location. Depending on the accuracy of the difference scheme, this require one or more dissipation operators. The accuracy of the difference approximation is chosen as high as possible within the computational stencil of the difference approximation of the system matrix. All dissipation operators used here are in the form

$$A_{2k} = -\Delta x P^{-1}\tilde{D}_k^T B \tilde{D}_k,$$

where P^{-1} is the diagonal norm of the first derivative as before, $\tilde{D}$ is an approximation of $(\Delta x)^k \partial^k / \partial x^k$ and B is a diagonal positive definite matrix. In most cases here, B is replaced by a single constant β. An appropriate choice of dissipation constant results in an upwind scheme, suitable for problems where shocks evolve. For further reading about the design of artificial dissipation operators we refer to [12].

5.1 A scalar problem and constant coefficients

First consider the scalar problem given by

$$u_t + au_x = 0. \quad (48)$$

This problem is discretized in space with a second order central scheme and dissipation is added, which yields

$$u_t + (aD_0 + \beta\Delta x P^{-1}\tilde{D}_+\tilde{D}_-)u = 0. \tag{49}$$

Penalty terms for the boundary conditions are neglected in this analysis. By choosing β appropriately, the spatial operator will become an upwind operator. The upper or lower diagonal terms of the matrix interior cancel if

$$\frac{|a|}{2} - \beta\Delta x = 0 \Leftrightarrow \beta = \frac{|a|}{2\Delta x}. \tag{50}$$

5.2 A system of equations and constant coefficients

We begin by considering a constant matrix A. In order to find the required dissipation operator, the system is diagonalized as in section 2.5. Let Λ denote a diagonal matrix where the entries are the eigenvalues of $H^{-1}A$ for all the discretization points. Then the discretized conservative system with dissipation is given by

$$\begin{aligned} w_t + \frac{1}{2}(P^{-1}Q \otimes I)\Lambda w &= -\Delta x\beta(P^{-1}\tilde{D}^T\tilde{D} \otimes I)\left|\Lambda\right|_{est} w \\ \Leftrightarrow w_t + (P^{-1} \otimes I)&\left[\frac{1}{2}(Q \otimes I)\Lambda + \Delta x\beta(\tilde{D}^T\tilde{D} \otimes I)\left|\Lambda\right|_{est}\right] w = 0. \end{aligned} \tag{51}$$

The diagonal matrix $\left|\Lambda\right|_{est}$ is an estimate of the absolute values of the eigenvalues and chosen in order to cancel matrix entries (either below or above the main diagonal). For a second order accurate difference operator of the form $P^{-1}Q$, an upwind scheme is obtained if we have

$$-\frac{1}{4} + \beta\Delta x = 0 \Leftrightarrow \beta = \frac{1}{4\Delta x}. \tag{52}$$

In reality, Λ is dependent on $u(x)$ so there is no global $\left|\Lambda\right|_{est}$ that fulfills the condition unless u is constant. To deal with varying Λ one can set

$$\left|\Lambda\right|_{est} = \lambda_{max} I,\ \lambda_{max} = \max\left|\lambda(x)\right|, \tag{53}$$

where λ denotes the components of Λ.

5.3 Dissipation for the 4th order difference approximation

With the aim of increasing accuracy, the second order accurate difference scheme is replaced by a fourth order accurate difference operator approximating the first order derivative with a five-point-scheme in the interior of the domain. This scheme requires two dissipation operators to make the overall difference operator one-sided

close to the shock or transition region. The fourth order difference approximation in the interior is given by

$$u_x \approx \frac{8u_{m+1} - u_{m+2} - 8u_{m-1} + u_{m-2}}{12h}. \tag{54}$$

Assuming an accurate estimate of $|\Lambda|_{est}$, we now choose β_1 and β_2 in

$$w_t + (P^{-1} \otimes I) \left[\frac{1}{2}(Q \otimes I)\Lambda w + \left(\Delta x(\beta_1 \tilde{D_1}^T \tilde{D_1} + \beta_2 \tilde{D_2}^T \tilde{D_2}) \otimes I \right) |\Lambda| \right] w = 0, \tag{55}$$

in order to get an upwind scheme. For each interior point u_m we have a total difference operator

$$\begin{aligned} Lu_m = \Bigg[\frac{\lambda_j}{2\Delta x} \begin{pmatrix} \frac{1}{12} & -\frac{2}{3} & 0 & \frac{2}{3} & -\frac{1}{12} \end{pmatrix} + \beta_1 |\lambda_j| \begin{pmatrix} 1 & -4 & 6 & -4 & 1 \end{pmatrix} + \\ + \beta_2 |\lambda_j| \begin{pmatrix} 0 & -1 & 2 & -1 & 0 \end{pmatrix} \Bigg] \begin{pmatrix} u_{m-2} \\ u_{m-1} \\ u_m \\ u_{m+1} \\ u_{m+2} \end{pmatrix}. \end{aligned} \tag{56}$$

The operator is one-sided with the dissipation coefficients $\beta_1 = \frac{1}{24\Delta x}$ and $\beta_2 = \frac{1}{6\Delta x}$. (54) can now be written

$$w_t + (P^{-1} \otimes I) \left[\frac{1}{2}(Q \otimes I)\Lambda + \left(\left(\frac{1}{6} \tilde{D_1}^T \tilde{D_1} + \frac{1}{24} \tilde{D_2}^T \tilde{D_2} \right) \otimes I \right) |\Lambda| \right] w = 0. \tag{57}$$

The difficulty lies in estimating Λ, which can again be replaced by estimating the largest eigenvalue only. For the system of equations generated by polynomial chaos expansion of Burgers' equation, max $|\lambda|$ is not known. Since the only non-zero polynomial coefficients on the boundaries are u_0 and u_1 and since the polynomial chaos expansion converges in the L_2 sense, a reasonable approximation of the maximum eigenvalue of $H^{-1}\Lambda$ is

$$|\lambda|_{max} \approx |u_0| + M |u_1|, \tag{58}$$

where M is the order of polynomial chaos expansion. This estimate is justified by the eigenvalue analysis performed earlier as well as by experimental results. The dissipation operators used in the simulations are therefore

$$A_2 = -\frac{(|u_0| + M |u_1|)}{6} P^{-1} \tilde{D_1} B_1 \tilde{D_1} \tag{59}$$

$$A_4 = -\frac{(|u_0| + M |u_1|)}{24} P^{-1} \tilde{D_2} B_2 \tilde{D_2} \tag{60}$$

where B_1 and B_2 are non-negative diagonal matrices.

6 Time integration

The increase in simulation cost associated with higher order systems is due to a number of factors. The size of the system depends both on the number of terms in the truncated polynomial chaos expansion and the spatial mesh size.

For the Kronecker product $A \otimes B$ the relation

$$\lambda_{A \otimes B} = \lambda_A \lambda_B \tag{61}$$

holds. This enables a separate analysis of the eigenvalues corresponding to the polynomial chaos expansion and the eigenvalues corresponding to the spatial discretization. Assuming constant coefficients, we have

$$w_t + (P^{-1}T \otimes \Lambda)w = 0, \tag{62}$$

where $P^{-1}T$ is a spatial operator of the form derived in (57). For the spectral radius ρ, we have $\rho(\Lambda_g) \leq \rho(I \otimes \Lambda_{max})$ and thus the maximum system eigenvalue is limited by

$$\lambda_{max} \leq \max\lambda_{P^{-1}T} \max\lambda_{H^{-1}A}. \tag{63}$$

The estimate (63) will be used in order to obtain estimates of the time step constraint.

6.1 Eigenvalue approximation

Analytic eigenvalues for the system matrix $H^{-1}A$ can only be obtained for a small number of polynomial chaos coefficients and therefore approximations are needed. Even though most eigenvalues of interest in this report can be calculated exactly for every particular case, a general estimate is of interest. The approximation of the largest eigenvalue of the scaled system matrix $H^{-1}A$ is calculated from solution values on the boundaries, which are the only values known a priori. For smooth solutions with boundary conditions where the polynomial chaos coefficients u_i are equal to 0 for $i > 1$, the higher order coefficients tend to remain small compared to lower order coefficients (strong probabilistic convergence). For solutions where a shock is developing, higher order polynomial chaos coefficients might grow and the approximation of the largest eigenvalue based on boundary values is likely to be a less accurate estimate.

To get estimates of the eigenvalues, the system of equations can be written

$$u_t + H^{-1}\left(\sum_{i=0}^{M} A_i(u_i)\right) u_x = 0, \tag{64}$$

where A is a linear combination of the polynomial chaos coefficients. We have

$$A(u) = \sum A_i(u_i) \tag{65}$$

and

$$A_i(u_i) = A_i u_i. \tag{66}$$

The eigenvalue approximation used here is given by

$$\max \lambda_{H^{-1}A} = \max \frac{x^T (H^{-1} \sum A_i u_i) x}{x^T x} \leq \sum \max \frac{x_i^T H^{-1} A_i x_i}{x_i^T x_i} |u_i| = \\ = \sum |u_i| \max |\lambda_i| . \tag{67}$$

Since $H^{-1}A_0(u_0) = u_0 I$, this approximation coincides with the exact eigenvalue for boundary value with $u_i = 0$ for $i > 1$. This can be seen by observing that if x_1 is an eigenvector with corresponding eigenvalue λ for the matrix $H^{-1}A_1$ then $H^{-1}A_1 x = \lambda x$ and

$$H^{-1}(A_1 u_1 + A_0 u_0)x = u_1 \lambda x + u_0 I x = (u_1 \lambda + u_0)x \tag{68}$$

so $u_1\lambda + u_0$ and x_1 are eigenvalue and eigenvector to the matrix $H^{-1}(A_0 u_0 + A_1 u_1) = H^{-1}A$. This shows that (58) is an appropriate eigenvalue approximation for problems where only u_0 and u_1 are non-zero on the boundaries.

For a given boundary condition, the maximum eigenvalue of A_0 corresponding to the deterministic part of the condition does not change with increasing number of polynomial chaos coefficients. However, the largest eigenvalue contribution from A_1 grows with the number of polynomial chaos coefficients. Consider again the perturbed sine wave in (32). Since the expected value is zero on the boundaries, the largest eigenvalue is estimated from u_1 only. The inverse of the largest eigenvalue is proportional to the maximum time step.

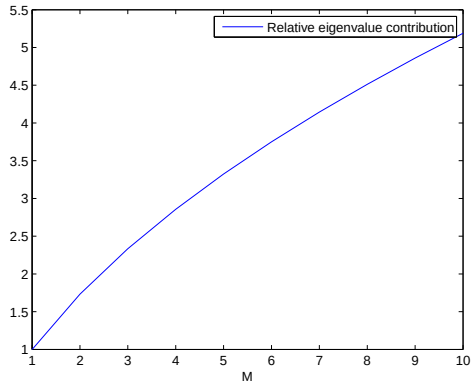

Figure 2: Maximum eigenvalues of $H^{-1}A = H^{-1}A_1$ at the boundaries at $t = 0$. for the perturbed sine wave.

The eigenvalue approximation (58) is in general of the same order of magnitude as the largest eigenvalue in the interior of the domain but might have to be adjusted to remove all oscillations. The exact value is problem specific and an estimate based on the interior values requires knowledge about the solution of the problem.

One way of getting the optimal dissipation operator is to perform a test simulation on a rough grid where the strength of the dissipation operator is based on the boundary value. If the solution is oscillatory, the dissipation should be increased according to the maximum eigenvalue corresponding to this solution. When the oscillations disappear the grid can be refined for the actual simulation.

An example may illustrate this method. Consider the initial and boundary conditions in the problem given by

$$
\begin{aligned}
&u(0,t) = 2 + 0.5\xi,\ u(1,t) = -2 \\
&u(x,0) = 2(1-2x) + 0.5\xi(1-x) \\
&\xi \in N(0,1)
\end{aligned}
$$

The eigenvalues of the boundaries of the system can be evaluated and used as an estimate of the largest eigenvalue over the domain. We use the eigenvalue approximation (58) to get $|\lambda|_{max} = 4$, which is used in the test simulation. At $t = 0$ this is indeed the largest eigenvalue throughout the domain. However, this problem is an example of the supersensitivity problem mentioned in the introduction and variability increases with time. The solution is bounded but oscillating and can be used to get an improved estimate of the largest eigenvalue. With this eigenvalue estimate, $|\lambda|_{max} = 9$, the oscillations disappear, see Figure 4.

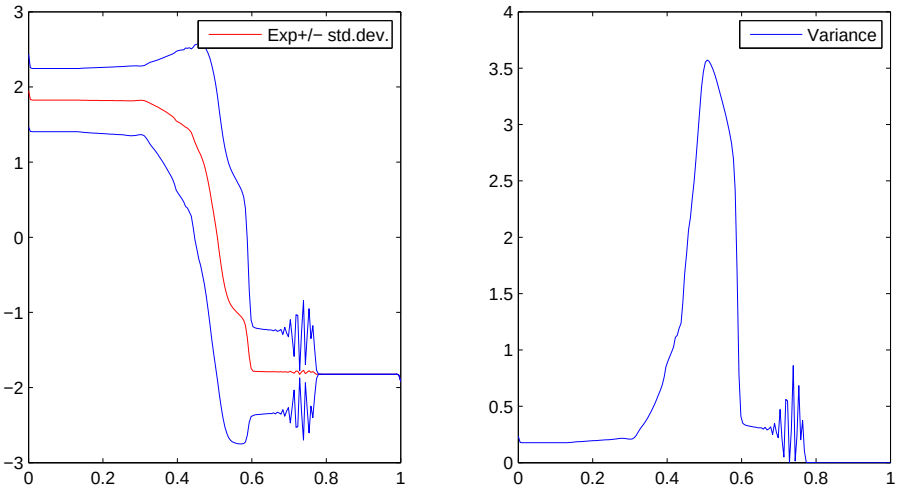

Figure 3: One-sided uncertainty, oscillating solution. $E[u] \pm \sigma$ (left) and σ^2 (right). $M = 4$ at $t = 0.25$.

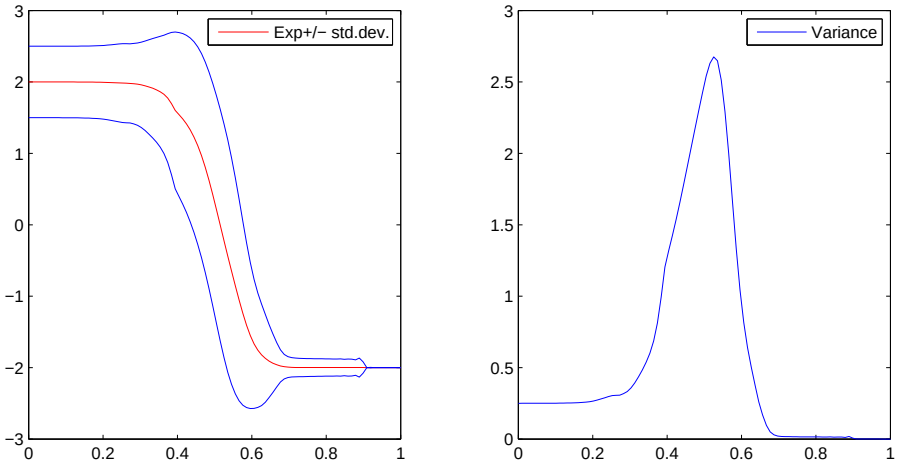

Figure 4: One-sided uncertainty. $E[u] \pm \sigma$ (left) and σ^2 (right). $M = 4$ at $t = 0.25$.

Note that a relatively large number of polynomial chaos coefficients is needed for accuracy, see Table 3.

M	0	1	2	3	4	5	6
$\|\epsilon_{Exp}\|$	0.460	0.0202	0.0149	0.00842	0.00522	0.00288	0.00181
$\|\epsilon_{Var}\|$	0.0942	0.0688	0.0316	0.0335	0.0212	0.0106	0.00679

Table 3: Convergence for the solution in Figure 4. u_{ref} for $M = 7$

Remark: The dissipation operator is not optimal for every choice of M because of approximations of eigenvalues and therefore the convergence is not monotone.

6.2 Choice of time step

The complete problem can schematically be written

$$u_t = (T \otimes H^{-1}A)u + \Sigma(u - g). \tag{69}$$

Ideally, the construction of T by means of adding dissipation and penalty terms should be such that all the real parts of the eigenvalues are non-positive.

By diagonalizing (69) we obtain a decoupled system of the form

$$w_t = \Lambda w + G(g).$$

We can now analyze the stability by considering the model problem $u_t = \lambda u$. The stability boundary for Euler forward is given by the complex roots of $g_a = 1 + \lambda\Delta t = e^{i\theta}$ for arbitrary real θ. Similarly, for the fourth order Runge-Kutta with

more Taylor expansion coefficients included in the time derivative approximation, the boundary of the stability region consists of the roots of

$$g_a = 1 + \lambda\Delta t + \frac{(\lambda\Delta t)^2}{2} + \frac{(\lambda\Delta t)^3}{3!} + \frac{(\lambda\Delta t)^4}{4!} = e^{i\theta}.$$

Stability is obtained by choosing Δt such that $|g_a| \leq 1$ where g_a is the amplification for the time step, $u^{n+1} = g_a u^n$.

The stability of the system is primarily governed by the system matrix entries corresponding to the boundaries and the shock location. These regions and the parts of the domain that are between them have different impacts on the location of $\lambda\Delta t$ within the stability region. The most critical issue in terms of stability is not the theoretical upper limit on the time step but the occurence of small positive eigenvalues of the system matrix, leading to instability for the explicit Euler as well as for the fourth order Runge-Kutta method.

The penalty matrix Σ also affects the eigenvalues of the system matrix. Σ should be chosen strong enough to force the boundary values towards the given condition but sufficiently weak so that the system does not become too stiff. There is a tradeoff between these requirements.

The relation

$$\max\lambda_{\text{system}} = (\max\lambda_D)(\max\lambda_{H^{-1}A})$$

implies that the largest eigenvalues of the space discretization operator D and the weighted polynomial chaos matrix $H^{-1}A$ both contribute to the constraint of the time step.

7 Theoretical results and interpretation

7.1 Analysis of characteristics: disturbed cosine wave

In this section, the characteristics of the stochastic Burgers' equation with $M = 1$ (truncated to 2×2 system) will be investigated to give a qualitative measure of the time development of the solution. The system is given by

$$\begin{pmatrix} u_0 \\ u_1 \end{pmatrix}_t + \begin{pmatrix} u_0 & u_1 \\ u_1 & u_0 \end{pmatrix} \begin{pmatrix} u_0 \\ u_1 \end{pmatrix}_x = 0. \tag{70}$$

Eigenvalues: $\lambda = u_0 \pm u_1$; eigenvectors: $x_1 = \begin{pmatrix} 1 \\ 1 \end{pmatrix}$ $x_2 = \begin{pmatrix} 1 \\ -1 \end{pmatrix}$.

The diagonal form of the stochastic Burgers' equation is

$$\frac{1}{\sqrt{2}} \begin{pmatrix} u_0 + u_1 \\ u_0 - u_1 \end{pmatrix}_t + \begin{pmatrix} u_0 + u_1 & 0 \\ 0 & u_0 - u_1 \end{pmatrix} \frac{1}{\sqrt{2}} \begin{pmatrix} u_0 + u_1 \\ u_0 - u_1 \end{pmatrix}_x = 0. \tag{71}$$

With $w_1 = u_0 + u_1$ and $w_2 = u_0 - u_1$, (71) can be rewritten

$$\begin{pmatrix} w_1 \\ w_2 \end{pmatrix}_t + \begin{pmatrix} w_1 & 0 \\ 0 & w_2 \end{pmatrix} \begin{pmatrix} w_1 \\ w_2 \end{pmatrix}_x = 0. \tag{72}$$

Consider first the slightly different initial-boundary value problems with a disturbed cosine wave stated below.

Ex 1.1

$u(0,t) = 1 + 0.1\xi$
$u(1,t) = -(1 + 0.1\xi)$
$u(x,0) = cos(\pi x) + 0.1\xi(1 - 2x)$
$\xi \in N(0,1)$

Ex 1.2

$u(0,t) = 1 + 0.1\xi$
$u(1,t) = -1 + 0.1\xi$
$u(x,0) = cos(\pi x) + 0.1\xi$
$\xi \in N(0,1)$

The problems are similar in terms of boundary expected value and variance, but the difference in sign in front of the stochastic variable completely change the behavior over time. Note that the difference in initial variance in the interior of the domain does not explain this difference entirely; this has been checked by varying the initial function.

The polynomial chaos coefficients of the boundaries are given by

$$\left.\begin{matrix} u_0 = 1 \\ u_1 = 0.1 \end{matrix}\right\} x = 0, \quad \left.\begin{matrix} u_0 = -1 \\ u_1 = -0.1 \end{matrix}\right\} x = 1$$

and

$$\left.\begin{matrix} u_0 = 1 \\ u_1 = 0.1 \end{matrix}\right\} x = 0, \quad \left.\begin{matrix} u_0 = -1 \\ u_1 = 0.1 \end{matrix}\right\} x = 1$$

respectively.

Higher order coefficients are zero at the boundaries. In the analysis of characteristics, the system is truncated to $M = 1$. The sign of the coefficients is crucial. In both cases the expected values as well as the variance are the same. However, in the first case both characteristics will give rise to a shock at $x = 0.5$ and result in variance going towards 0 at the shock location. In the second case the characteristics will give rise to shocks at $x = 0.45$ and $x = 0.55$ respectively. The variance will peak between these points.

The expected value at each point is the mean of the characteristics, $E(u) = u_0 = \frac{w_1+w_2}{2}$ and the variance depends on the distance between the characteristics, $Var(u) = u_1^2 = \left(\frac{w_1-w_2}{2}\right)^2$.

Experimental results agree with the analysis of characteristics. Compare the analysis of characteristics for the two examples with $M = 1$ in Figure 5 to the solutions of the same problems for $M = 6$ in Figure 6. In Ex 1.1, the characteristics coincide at $x = 0.5$, corresponding to the variance approaching zero at $x = 0.5$ in Figure 6a. The gap between the characteristics at $x = 0.5$ in Figure 5b corresponds to the variance peak at this location in 6b.

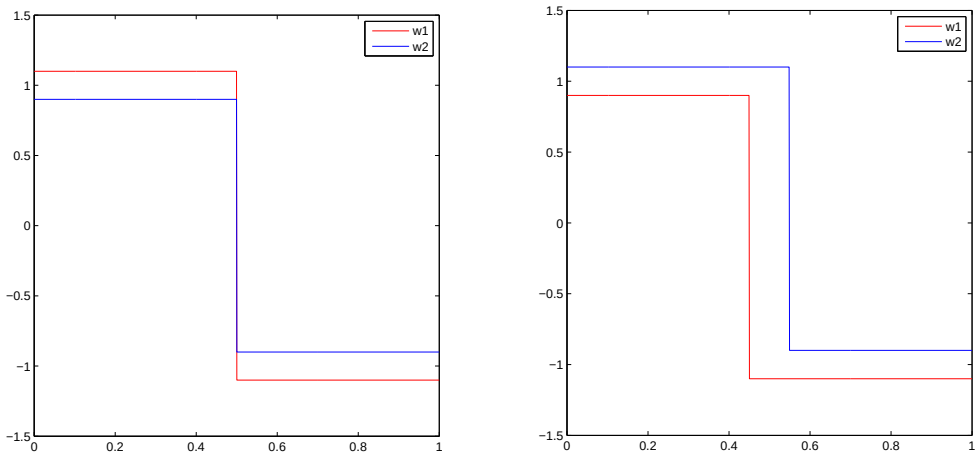

(a) Ex 1.1. Variance approach zero at the shock location

(b) Ex 1.2. Variance peaks at the shock location

Figure 5: Characteristics of the two perturbed cosine waves (Ex 1.1 and Ex 1.2) for $M = 1$.

The modeling of uncertainty for this kind of symmetric problems will have an impact on other design parameters of the simulation. Although the sign of the stochastic variable does not affect neither expected value nor variance of the initial and boundary conditions, it will affect the simulation. For instance, the amount of dissipation is affected by this choice. This can be seen in Figure 6 below, showing the two cases at time $t = 0.3$ for $M = 6$. Larger maximum variance require more artificial dissipation.

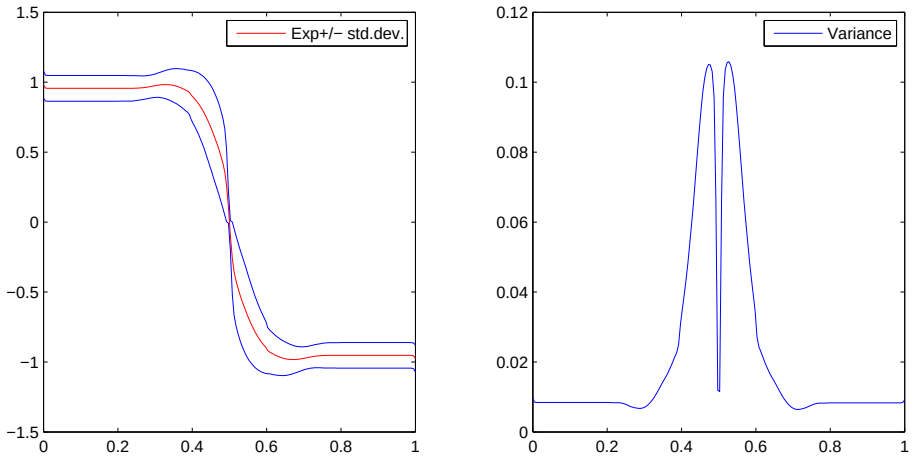

(a) Ex 1.1. Symmetric boundary conditions.

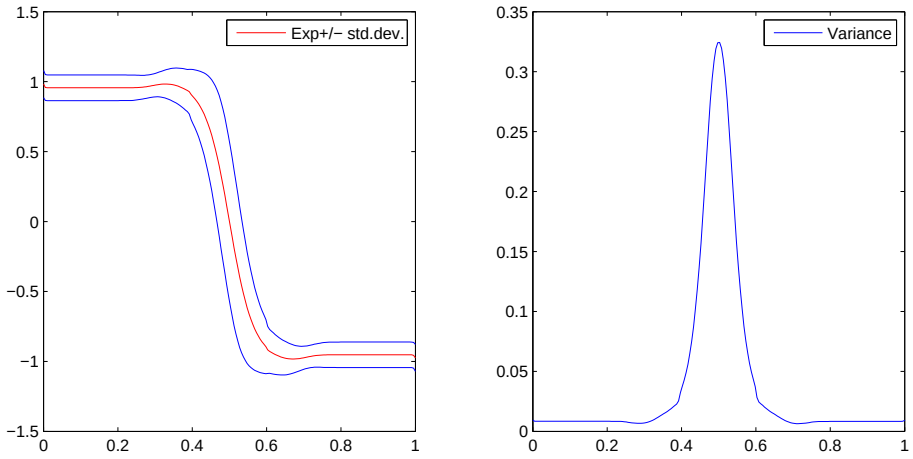

(b) Ex 1.2. Uniform initial variance.

Figure 6: Development of variance of the perturbed cosine wave.

The convergence of the solution of the problems in Figure 6 is shown in Table 4.

M	0	1	2	3	4	5	6
$\|\epsilon_{Exp}\|$	0.0273	0.0172	0.00637	0.00522	0.00292	0.00262	0.00110
$\|\epsilon_{Var}\|$	0.0410	0.0166	0.00594	0.00433	0.00231	0.00191	0.00117
$\|\epsilon_{Exp}\|$	0.0538	0.0209	0.0115	0.00546	0.00472	0.00276	0.00257
$\|\epsilon_{Var}\|$	0.0967	0.0336	0.0147	0.00904	0.00579	0.00373	0.00365

Table 4: Convergence for the solution to Ex 1.1 (above) and Ex 1.2 (below). u_{ref} for $M = 6$, $m = 400$, $t = 0.3$.

The lower variance in Ex 1.1 requires less artificial dissipation in order to maintain stability than is needed in Ex 1.2. In the figure the same amount of dissipation has been used in both simulations.

The system used for analysis of characteristics is truncated to $M = 1$, but the conclusions about the qualitative behavior holds for higher order systems. Including more polynomial chaos coefficients would give a smoother solution. Observe the qualitative similarities between the solutions in Figure 5 and Figure 6. Regardless of the truncation of polynomial chaos coefficients, the variance approaches 0 at the shock location in Ex 1.1. At the shock location in Ex 1.2 the variance reaches a maximum that will spread towards the boundaries and annihilate the shock effect.

The observation that the same boundary and initial expected value and variance can give totally different solutions indicates that knowledge about expected value and variance is insufficient to obtain a unique solution. The information content of the polynomial chaos coefficients is indeed greater than that of the expected values and the variance.

The analysis of characteristics further show that the problem could be partitioned into several phases of development, depending on the speeds of the characteristics. Consider again the boundary conditions of Ex 1.1 and Ex 1.2 but for generality assume zero flow in the interior at time $t = 0$. The solution for $M = 1$ before the meeting of the characteristics from the left and the right are shown in Figure 7. With more polynomial chaos coefficients, the edges of the solution will disappear. At time $t = 0.5$, the solutions to the two problems are still similar, with two variance peaks at the shocks that are traveling towards the middle of the domain.

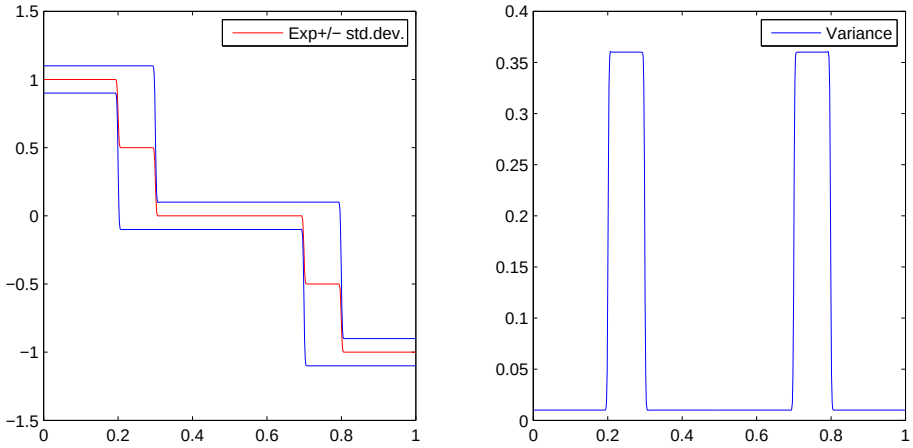

(a) Uniform boundary condition, $u_1 = 0.1$.

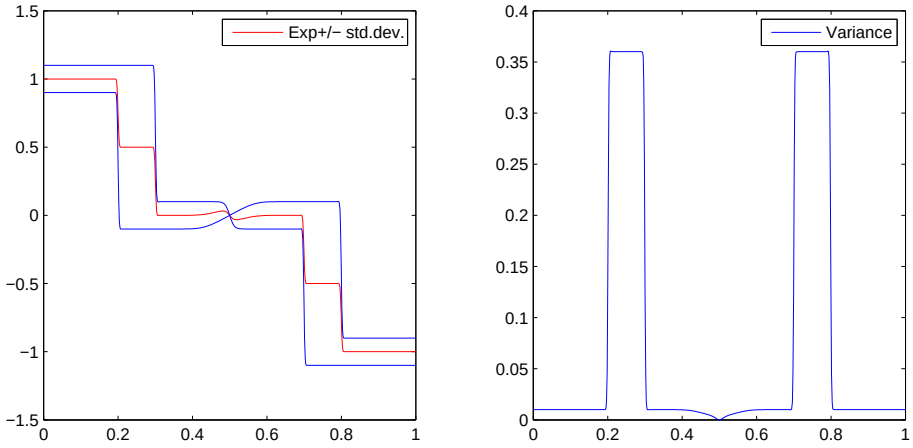

(b) Symmetric boundary condition, $u_1 = \pm 0.1$.

Figure 7: Solution with flow from both boundaries at $t = 0.5$, $M = 1$.

Asymptotically in time, the symmetric problem (Ex. 1.1) will result in a stationary shock. The variance will equal the initial boundary variance except for a

peak at the very location of the shock. As can be seen in Figure 8 b, the asymptotic behavior of the problem with uniform uncertainty is not consistent with the static boundary conditions stated in the problem formulation. The characteristics are transported from one boundary to the other, thus changing the boundary conditions. The boundary conditions of Ex 1.2 must therefore be time-dependent.

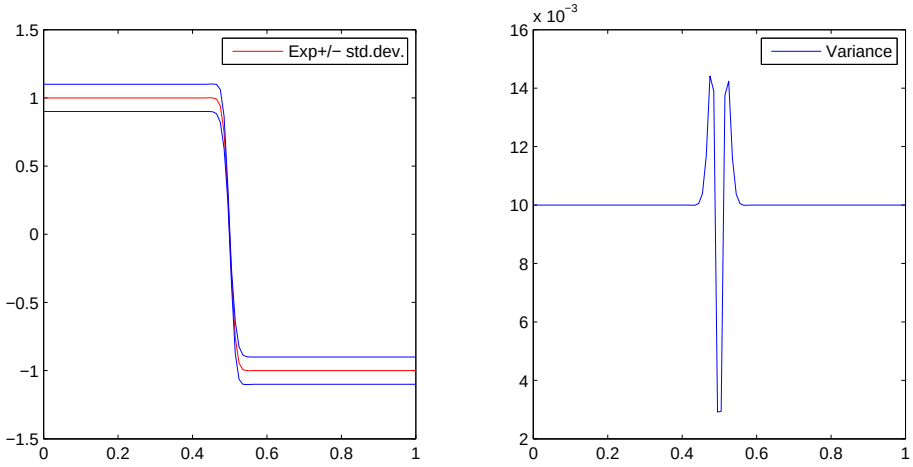

(a) Uniform boundary condition, $u_1 = 0.1$

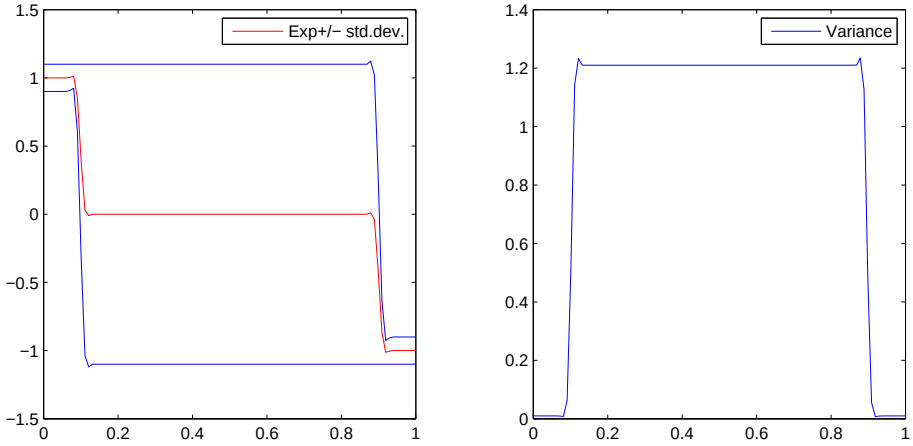

(b) Symmetric boundary condition, $u_1 = \pm 0.1$

Figure 8: Solution for flow from both boundaries at $t = 4$, $M = 1$.

7.2 Analysis of characteristics: disturbed sine wave

Analysis of characteristics is performed for the perturbed sine wave (32). As a comparison the variance is also modeled as in the case of the cosine wave with opposite signs of u_1 on the boundaries.

A transition layer develops where the characteristics meet but because of the boundary conditions, the energy of the system decays and the flow asymptotically goes to zero througout the domain, see Figure 9. As for the perturbed cosine wave, opposite signs of the stochastic variable at the boundaries result in decreasing variance in the interior. With constant initial uncertainty over the domain, the variance close to the transition layer will grow to a certain value and then decrease as the expected flow goes to zero throughout the domain.

In Figure 9, the perturbed sine wave is modeled with standard deviation $\sigma = 0.2$ and shown at $t = 0.25$. The energy of the system will decay no matter of the sign of the stochastic variable.

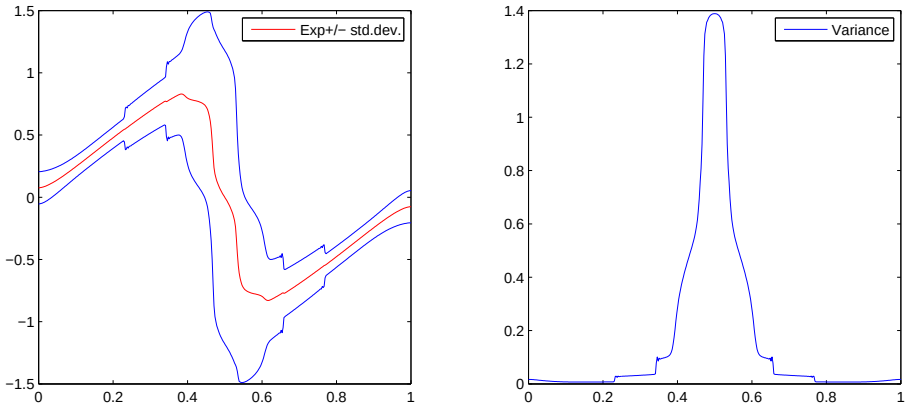

(a) Perturbed sine wave. $u_1 = 0.2$ everywhere.

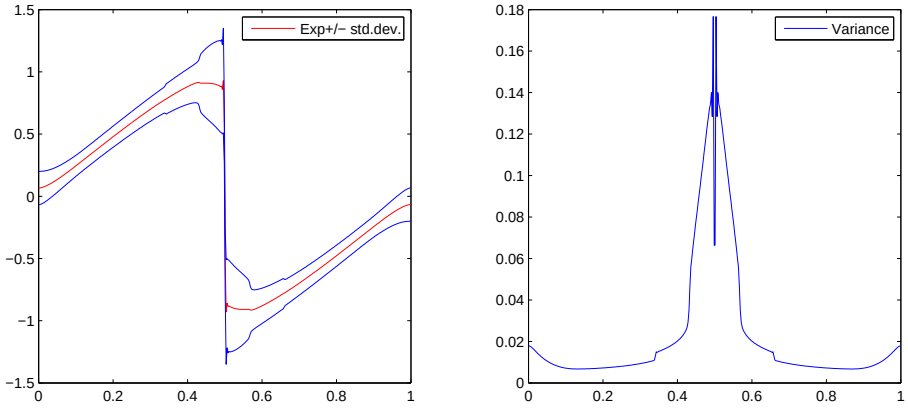

(b) Perturbed sine wave. $u_1 = 0.2$ at $x = 0$, $u_1 = -0.2$ at $x = 1$.

Figure 9: Perturbed sine waves. $M = 5$; $dt = 0.0002$; $dx = 1/400$.

Note that the sharp edges appearing in the variance are not due to oscillations but a correct modeling of the solution for a truncated polynomial chaos series. The edges disappear with increasing M.

7.3 The influence of variance on the smoothness of the expected value

Consider the equation for the expected value u_0,

$$\frac{\partial u_0}{\partial t} + u_0 \frac{\partial u_0}{\partial x} = -\sum_{i=1}^{M} i! u_i \frac{\partial u_i}{\partial x}. \tag{73}$$

With no uncertainty in the boundary conditions, (73) reduces to the deterministic Burgers' equation for u_0. Inflow at both boundaries will result in a shock. However, as shown in Figure 6, uncertain boundary conditions will result in a smooth transition layer instead of a shock in u_0. This suggests that while preserving the original conditions for the expected flow, a deterministic problem describing the development of a shock can be augmented with stochastic conditions which makes the problem well-behaved (derivatives existing everywhere). The figures below both show the perturbed cosine wave at $t = 0.3$ with standard deviation $\sigma = 0.1$ (a) and $\sigma = 0.3$ (b).

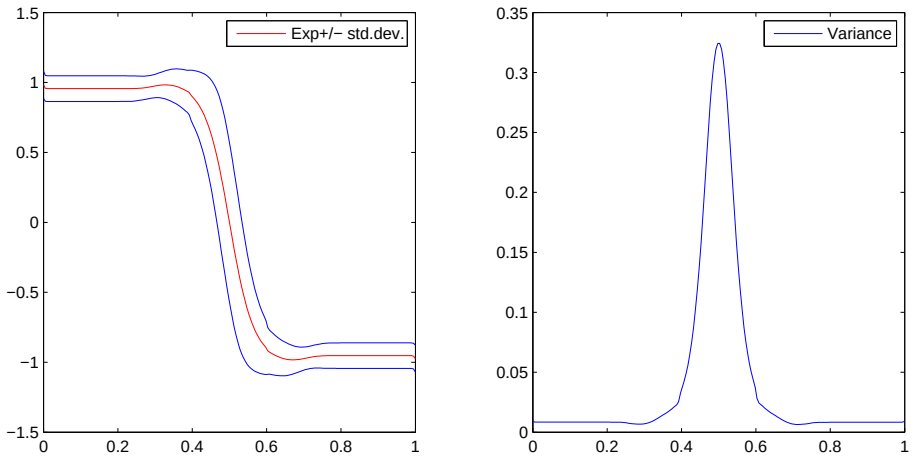

(a) $\sigma = 0.1$

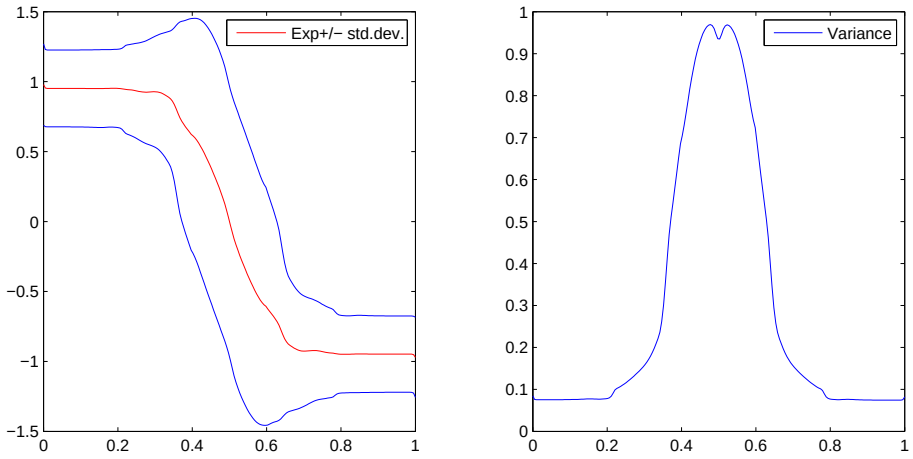

(b) $\sigma = 0.3$

Figure 10: Development of variance for the perturbed cosine wave at $t = 0.3$

The explanation to the different transition behavior can be found by considering the characteristics. For a system with inflow at both boundaries and truncated to M polynomial chaos coefficients, there will be M system eigenvalues. If there is no uncertainty, all eigenvalues are equal, $\lambda = u_0$ and one shock will develop. With non-zero variance there will be M distinct eigenvalues and thus M characteristics traveling with different speeds. At a fixed time t, the characteristics will give rise to shocks at different locations and the expected value curve will therefore contain the same number of discontinuities as there are distinct eigenvalues. When $M \to \infty$, the magnitude of these shocks goes to zero and the expected value curve becomes smooth.

8 Summary and conclusions

The polynomial chaos approach and stochastic Galerkin methods are used to solve the stochastic Burgers' equation with finite difference methods. Stable difference schemes are obtained by the use of artificial dissipation, difference operators satisfying the summation by parts property and a weak imposition of boundary conditions.

The problem is shown to be well-posed. Even though the solution to the stochastic Burgers' equation is discontinuous for a particular value of the stochastic variable, the polynomial chaos coefficient functions are generally continuous.

The eigenvalues and characteristics are analyzed to get a qualitative description of the solution over time. For the truncated system with $M = 1$, the variance and expected value can be estimated directly from the two characteristics. This is useful in estimating the largest eigenvalue of the system matrix.

The deterministic inviscid Burgers' equation is shown to be a particular case of

the stochastic Burgers' equation, with zero variance throughout the domain. Only one simulation is needed to get a probabilistic solution, but the cost increases with the number of polynomial chaos coefficients.

A Appendix

A.1 Table of probabilistic Hermite polynomials

The first twelve Hermite polynomials are given below.
$H_0 = 1$
$H_1 = x$
$H_2 = x^2 - 1$
$H_3 = x^3 - 3x$
$H_4 = x^4 - 6x^2 + 3$
$H_5 = x^5 - 10x^3 + 15x$
$H_6 = x^6 - 15x^4 + 45x^2 - 15$
$H_7 = x^7 - 21x^5 + 105x^3 - 105x$
$H_8 = x^8 - 28x^6 + 210x^4 - 420x^2 + 105$
$H_9 = x^9 - 36x^7 + 378x^5 - 1260x^3 + 945x$
$H_{10} = x^{10} - 45x^8 + 630x^6 - 3150x^4 + 4725x^2 - 945$
$H_{11} = x^{11} - 55x^9 + 990x^7 - 6930x^5 + 17325x^3 - 10395x$
$H_{12} = x^{12} - 66x^{10} + 1485x^8 - 13860x^6 + 51975x^4 - 62370x^2 + 10395$

Higher order polynomials can be calculated by

$$H_{n+1}(\xi) = \xi H(\xi) - nH_{n-1}(\xi)$$

References

[1] A.H.S. Ang and W.H. Tang. *Probability Concepts in Engineering Planning and Design, Volume I, Basic Principles*. Wiley, first edition, 1975.

[2] Philip S. Beran, Chris L. Pettit, and Daniel R. Millman. Uncertainty quantification of limit-cycle oscillations. *J. Comput. Phys.*, 217(1):217–247, 2006.

[3] Jane M. Booker, Timothy J. Ross, Brian J. Reardon, Francois M. Hemez, Mark C. Anderson, Scott W. Doebling, and Cliff A. Joslyn. An engineering perspective on uq for validation, reliability and certification. *Foundations 04 Workshop for Verification, Validation, and Accreditation (VVA) in the 21st Century*, October 2004.

[4] R.H. Cameron and W.T. Martin. The Orthogonal Development of Non-Linear Functionals in Series of Fourier-Hermite Functionals. *The Annals of Mathematics*, 48(2):385–392, April 1947.

[5] Mark H. Carpenter, Jan Nordström, and David Gottlieb. A stable and conservative interface treatment of arbitrary spatial accuracy. *J. Comput. Phys.*, 148(2):341–365, 1999.

[6] Qian-Yong Chen, David Gottlieb, and Jan S. Hesthaven. Uncertainty analysis for the steady-state flows in a dual throat nozzle. *J. Comput. Phys.*, 204(1):378–398, 2005.

[7] Mike Christie, Vasily Demyanov, and Demet Erbas. Uncertainty quantification for porous media flows. *J. Comput. Phys.*, 217(1):143–158, 2006.

[8] C.F. van Loan G. H. Golub. *Matrix Computations*. Johns Hopkins University Press, second edition, 1989.

[9] Beril Gustafsson, Heinz-Otto Kreiss, and Joseph Oliger. *Time dependent problems and difference methods*. Wiley, first edition, 1995.

[10] Thomas Y. Hou, Wuan Luo, Boris Rozovskii, and Hao-Min Zhou. Wiener chaos expansions and numerical solutions of randomly forced equations of fluid mechanics. *J. Comput. Phys.*, 216(2):687–706, 2006.

[11] M Loève. *Probability Theory*. Springer-Verlag, fourth edition, 1977.

[12] Ken Mattsson, Magnus Svärd, and Jan Nordström. Stable and accurate artificial dissipation. *Journal of Scientific Computing*, 21(1):57–79, August 2004.

[13] Jan Nordström. Conservative finite difference formulations, variable coefficients, energy estimates and artificial dissipation. *J. Sci. Comput.*, 29(3):375–404, 2006.

[14] Jan Nordström and Mark H. Carpenter. Boundary and interface conditions for high-order finite-difference methods applied to the Euler and Navier-Stokes equations. *J. Comput. Phys.*, 148(2):621–645, 1999.

[15] Jan Nordström and Mark H. Carpenter. High-order finite difference methods, multidimensional linear problems, and curvilinear coordinates. *J. Comput. Phys.*, 173(1):149–174, 2001.

[16] C.L. Pettit and P.S. Beran. Spectral and multiresolution Wiener expansions of oscillatory stochastic processes. *Journal of Sound and Vibration*, pages 752–779, 2006.

[17] S. Poroseva, J. Letschert, and M. Y. Hussaini. Uncertainty Quantification in Hurricane Path Forecasts using Evidence Theory. *APS Meeting Abstracts*, pages B1+, November 2005.

[18] Matthew T. Reagan, Habib N. Najm, Roger G. Ghanem, and Omar M. Knio. Uncertainty quantification in reacting-flow simulations through non-intrusive spectral projection. *Combustion and Flame*, 2003.

[19] Bo Strand. Summation by parts for finite difference approximations for d/dx. *J. Comput. Phys.*, 110(1):47–67, 1994.

[20] Gabor Szegö. *Orthogonal Polynomials*. American Mathematical Society, fourth edition, 1975.

[21] Xiaoliang Wan and George Em Karniadakis. Long-term behavior of polynomial chaos in stochastic flow simulations. *Computer methods in applied mechanics and engineering*, pages 5582–5596, August 2006.

[22] Norbert Wiener. The homogeneous chaos. *American Journal of Mathematics*, 60(4):897–936, October 1938.

[23] Jeroen A. S. Witteveen, Sunetra Sarkar, and Hester Bijl. Modeling physical uncertainties in dynamic stall induced fluid-structure interaction of turbine blades using arbitrary polynomial chaos. *Comput. Struct.*, 85(11-14):866–878, 2007.

[24] Dongbin Xiu and George Em Karniadakis. The wiener–askey polynomial chaos for stochastic differential equations. *SIAM J. Sci. Comput.*, 24(2):619–644, 2002.

[25] Dongbin Xiu and George Em Karniadakis. Modeling uncertainty in flow simulations via generalized polynomial chaos. *Journal of Computational Physics*, pages 137–167, 2003.

[26] Dongbin Xiu and George Em Karniadakis. Supersensitivity due to uncertain boundary conditions. *International Journal for Numerical Methods in Engineering*, 61:2114–2138, October 2004.

[27] Y. Yu, M. Zhao, T. Lee, N. Pestieau, W. Bo, J. Glimm, and J. W. Grove. Uncertainty quantification for chaotic computational fluid dynamics. *J. Comput. Phys.*, 217(1):200–216, 2006.